Nuclear spin/parity dependent spectroscopy and predissociation dynamics in $v_{OH} = 2 \leftarrow 0$ overtone excited Ne–H_2O clusters: Theory and experiment

Michael P. Ziemkiewicz, Christian Pluetzer, Jérôme Loreau, Ad van der Avoird, and David J. Nesbitt

Citation: The Journal of Chemical Physics **147**, 214304 (2017);
View online: https://doi.org/10.1063/1.5001335
View Table of Contents: http://aip.scitation.org/toc/jcp/147/21
Published by the American Institute of Physics

Nuclear spin/parity dependent spectroscopy and predissociation dynamics in $v_{OH} = 2 \leftarrow 0$ overtone excited Ne–H_2O clusters: Theory and experiment

Michael P. Ziemkiewicz,[1] Christian Pluetzer,[2] Jérôme Loreau,[3] Ad van der Avoird,[4] and David J. Nesbitt[5]

[1]*Analog Devices, Inc., 14998 W. 6th Avenue #700, Golden, Colorado 80401, USA*
[2]*West Pharmaceuticals Services Deutschland GmbH & Co. KG, Stolberger Strasse 21-41, 52249 Eschweiler, Germany*
[3]*Université Libre de Bruxelles, Service de Chimie Quantique et Photophysique, 50 Ave. F. D. Roosevelt, CP 160/09, 1050 Brussels, Belgium*
[4]*Theoretical Chemistry, Institute for Molecules and Materials, Radboud University Nijmegen, Heyendaalseweg 135, 6525 AJ Nijmegen, The Netherlands*
[5]*JILA, National Institute of Standards and Technology, University of Colorado, and Department of Chemistry and Biochemistry, University of Colorado at Boulder, Boulder, Colorado 80309, USA*

(Received 23 August 2017; accepted 30 October 2017; published online 1 December 2017)

Vibrationally state selective overtone spectroscopy and state- and nuclear spin-dependent predissociation dynamics of weakly bound *ortho*- and *para*-Ne–H_2O complexes ($D_{0(ortho)} = 34.66\ cm^{-1}$ and $D_{0(para)} = 31.67\ cm^{-1}$) are reported, based on near-infrared excitation of van der Waals cluster bands correlating with $v_{OH} = 2 \leftarrow 0$ overtone transitions ($|02^-\rangle$ and $|02^+\rangle$) out of the *ortho* (1_{01}) and *para* (0_{00}) internal rotor states of the H_2O moiety. Quantum theoretical calculations for nuclear motion on a high level potential energy surface [CCSD(T)/VnZf12 (n = 3, 4)], corrected for basis set superposition error and extrapolated to the complete basis set (CBS) limit, are employed to successfully predict and assign Π–Σ, Σ–Σ, and Σ–Π infrared bands in the spectra, where Σ or Π represent approximate projections of the body-fixed H_2O angular momentum along the Ne–H_2O internuclear axis. IR-UV pump-probe experimental capabilities permit real-time measurements of the vibrational predissociation dynamics, which indicate facile intramolecular vibrational energy transfer from the H_2O $v_{OH} = 2$ overtone vibrations into the VdWs (van der Waals) dissociation coordinate on the $\tau_{prediss}$ = 15-25 ns time scale. Whereas all predicted strong transitions in the *ortho*-Ne–H_2O complexes are readily detected and assigned, vibrationally mediated photolysis spectra for the corresponding *para*-Ne–H_2O bands are surprisingly absent despite *ab initio* predictions of Q-branch intensities with S/N > 20-40. Such behavior signals the presence of highly selective nuclear spin *ortho-para* predissociation dynamics in the upper state, for which we offer a simple mechanism based on Ne-*atom mediated* intramolecular vibrational relaxation in the H_2O subunit (i.e., $|02^{\pm}\rangle \rightarrow \{|01^{\pm}\rangle;\ v_2 = 2\}$), which is confirmed by the *ab initio* energy level predictions and the nascent OH rotational (N), spin orbit ($\Pi_{1/2,3/2}$), and lambda doublet product distributions. *Published by AIP Publishing.* https://doi.org/10.1063/1.5001335

I. INTRODUCTION

Noncovalent interactions between molecules play a critical role in a variety of physical and chemical phenomena. These interactions govern, for example, critical aspects of solvation dynamics, hydrophobic effects, and molecular self-assembly, each of which provides strong motivation for developing a fundamental theoretical understanding of the underlying chemical physics.[1–5] This work focuses on a very simple example of non-covalent interaction in van der Waals dimers of H_2O with rare gas atoms, for which the equilibrium binding energies can vary dramatically from relatively robustly bound species[6] like Ar–H_2O (e.g., $D_0 \approx 100\ cm^{-1}$)[6–9] to fragile species[10] such as He–H_2O ($D_0 \approx 7\ cm^{-1}$).[9] Though such binding energies are typically small with respect to room temperature ($kT \approx 208\ cm^{-1}$), they nevertheless can be of major significance. For example, van der Waals interactions in hydrogen bound species (e.g., N_2–H_2O and H_2O–H_2O) have been speculated to facilitate sun-induced vibrational overtone chemistry in the Earth's atmosphere.[11–17] Weak interactions are now also thought to play a critical role in stabilizing pre-reactive complexes in the early stages of a chemical reaction,[15] as well as directly influencing structural isomer formation in a variety of low temperature environments such as supersonic jets,[17] noble gas matrices,[18] and doped helium nanodroplets.[19] Such interactions are also believed to control the solvation energetics of non-polar molecules in water[4] and thus influence the stability of clathrates under extreme pressure conditions.[20]

As introduced in a previous manuscript,[21] remarkably detailed insights into the intermolecular potential energy surfaces (PESs) associated with these interactions can be obtained via high resolution spectroscopy, made possible by the presence of a strong infrared chromophore (e.g., H_2O) in the rare

gas atom complex. In particular, the present work focuses specifically on Ne–H_2O, for which shallow internal rotation barriers in the potential energy surface can facilitate highly quantum mechanical, large amplitude effects. This system is of particular dynamical interest, as such weakly bound clusters permit quantum exploration over a significant fraction of the van der Waals potential energy surface even for the lowest internal rotor (*ortho* and *para*) nuclear spin isomers populated at supersonic jet temperatures. As a result, one might anticipate these systems to exhibit appreciable quantum effects due, for example, to *ortho/para* nuclear spin-dependent delocalization of the quantum wave functions.

There has been appreciable theoretical and experimental interest in the very lightest and most weakly bound van der Waals dimers of H_2O with He and H_2, particularly toward understanding transient dimer formation and collisional energy transfer dynamics in the interstellar medium.[22–24] There has also been much spectroscopic exploration of the heavier and much more strongly bound rare gas dimers of H_2O with Ar, Kr, and Xe, based on both direct absorption and vibrationally mediated photolysis techniques in the mid, near, and far infrared regions.[6,7,17,25–29] In contrast, however, there has been far less experimental work on Ne–H_2O complexes, for which the well depths ($D_0 \approx$ 32-36 cm^{-1}) and large amplitude internal rotor motion are clearly intermediate between He–H_2O and Ar–H_2O, yet also quite comparable to differences in the internal rotor energies of H_2O for the *ortho* vs. *para* nuclear spin manifolds.[3,6,8,9,30] For Ne–H_2O/D_2O clusters in the HOH/DOD fundamental bend region, there have been recent mid-infrared spectra reported which provided first high-resolution spectroscopic data on the bending manifold.[31] Interestingly, outside of our accompanying paper introducing this vibrationally mediated photolysis (VMP) work,[21] there have been no reports for Ne–H_2O spectra in either the OH stretch fundamental and/or the overtone region. In particular, there have been no studies whatsoever on quantum state-resolved rovibrational predissociation dynamics in these clusters, which represents a major focus of the present work.

To facilitate spectroscopic analysis of large amplitude motion in Ne–H_2O van der Waals complexes, potential energy surfaces have been calculated with MP2 theory,[3] with later refinements at the CCSD(T)/aug-cc-pVQZ level.[8,30] These studies have yielded estimates for equilibrium binding energies (i.e., excluding zero point motion in intermolecular degrees of freedom) of $D_e \approx 67$ cm^{-1} and a barrier to in-plane rotation[8] of $\approx$17 cm^{-1}. Theoretical studies by Sun *et al.*[32] reported an improved potential energy surface at the CCSD(T)/aug-cc-pVQZ level but also implemented multidimensional quantum calculations to extract many of the bound internal rotor states of Ne–H_2O for multiple Ne and O atom isotopomers. These early calculations facilitated simple fits of the *ab initio* energy levels to quasidiatomic rotational progressions, yielding estimates of rotational constants ($B \approx 0.142$ cm^{-1} and $D \approx 1.8 \times 10^{-5}$ cm^{-1}) for the ground state and already in fair agreement ($B = 0.13640$ cm^{-1} and $D = 1.63 \times 10^{-5}$ cm^{-1}) with results reported in high resolution spectroscopic studies by Li *et al.*[31] on the isotopically substituted Ne–D_2O system.

Previous rovibrational spectroscopy studies have been pursued on a number of related cluster systems, specifically H_2–H_2O,[22,24] Kr–H_2O,[27] and Xe–H_2O,[8] with particular attention paid to Ar–H_2O.[6,7,9,17,25,28] In-plane rotation of the H_2O molecule in Ar–H_2O is hindered by a 26 cm^{-1} barrier,[8] which constitutes only a relatively small perturbation with respect to its $D_e \approx 143$ cm^{-1} equilibrium binding energy. The presence of a small barrier permits largely free rotational motion but with sufficient torque in the molecular frame to make the angular momentum projection of H_2O (j_z) an approximately good quantum number, which, in the helicity decoupling approximation, is conventionally labeled as $K(J_{KaKc})$ [e.g., $\Sigma(1_{01})$ and $\Pi(1_{01})$] to indicate a specific asymmetric rotor wave function with $K = 0(\Sigma)$ or $1(\Pi)$ projection of J along the body-fixed intermolecular z-axis.[26,28] Built on such widely spaced internal rotor structure are also (i) progressions in the (rigorous) total angular momentum $\mathbf{J} = \mathbf{N} + \mathbf{j}$, which arise from the vector sum of internal rotor ($\mathbf{j}$) and end-over-end tumbling ($\mathbf{N}$) of the Ne–H_2O pseudodiatomic cluster and (ii) 1D vibrational excitation of van der Waals stretching quanta (n) along the center of mass axis, with (iii) rigorous labels for the H_2O nuclear spin state (*ortho*/*para*) and overall parity (e/f) of the total eigenfunction. In this work, we follow Brown *et al.*[33] by labeling states with the spectroscopic parity s, which is related to the true parity p by $p = s(-1)^J$ with $s = +1$ and $s = -1$ for e and f states, respectively. Due to a much smaller dissociation energy ($D_0 \approx$ 32-36 cm^{-1}), the number of energetically bound internal rotor/van der Waals states for Ne–H_2O is both small and yet still large enough to show interesting quantum dynamical effects.[21]

In addition to the rigorously bound states, there are also metastable "Feshbach resonance" states built on both inter- and intramolecular vibrations in the H_2O subunit that can be probed in the overtone IR action spectrum and are of special interest in the "ultracold collision" community.[9,34,35] This can be especially dramatic in Ne–H_2O rare gas clusters, where even lowest energy fundamental bending excitation of the H_2O moiety ($v_2 \approx 1600$ cm^{-1}) is already 50-fold greater than the dissociation limit. Such dramatic differences in inter- and intramolecular energy spacings translate semiclassically into a large detuning of time scales for non-resonant coupling into the dissociation coordinate. Due to the extreme dynamical metastability of these upper states, such weakly bound van der Waals systems still can in principle yield exceptionally high resolution (often Doppler/laser limited), rotationally structured infrared spectra, i.e., characteristics of many millions of vibrational periods prior to breaking the weak van der Waals bond.[7,36,37]

The final state distributions from such vibrationally mediated predissociation events also contain considerable information on the fragmentation dynamics, as elegantly demonstrated by Reisler and co-workers for a variety of internally excited hydrogen-bonded systems.[38] Indeed, one powerful advantage of the present IR-UV-UV triple resonance vibrationally mediated photolysis spectroscopic methods is that our experiment can be used to measure predissociation lifetimes *directly* for Ne–H_2O in the time domain by varying the IR pump and UV photolysis laser delays. This capability first yields access in these weakly bound systems to vibrational predissociation dynamics in real time as well as provides additional

rovibrational information on the recoiling H_2O species by virtue of UV laser induced fluorescence (LIF) distributions in the resulting OH photofragments.

The goal of the present work is a combined experimental and *ab initio* theoretical study of vibrationally mediated photolysis (VMP) $v_{OH} = 2 \leftarrow 0$ overtone spectroscopy and dynamics of the Ne–H_2O dimer. The organization of this paper will be as follows. Section II provides a brief overview of the experimental apparatus, followed in Sec. III by the description of the high level *ab initio* and quantum dynamical theoretical methods used to help assign and interpret the observed VMP spectra. Section IV contains a presentation of the key experimental results, specifically reporting infrared overtone absorption spectra in the $v_{OH} = 2 \leftarrow 0$ region for Ne–H_2O as well as the direct measurement of predissociation lifetimes for a series of H_2O internal rotor/vibrational upper states. Finally, in Sec. V, the results are explicitly discussed in comparison with "first principles" theoretical predictions and the dynamics of intramolecular vibrational relaxation (IVR) energy flow into the intermolecular coordinate, with results summarized in Sec. VI.

II. EXPERIMENTAL

The experimental apparatus for these VMP studies has been previously discussed in detail.[17,22,39,40] The Ne–H_2O complexes are formed in a slit supersonic expansion and encounter three spatially overlapped 8 ns laser pulses (IR-UV-UV) parallel to the long axis of the slit expansion to maximize the interaction path length (see Fig. 1). The first pulse from a tunable optical parametric oscillator (7210–7300 cm^{-1}, ~15 mJ, and $\Delta\nu_{laser} \approx 0.20$ cm^{-1} resolution) is tuned over the $v_{OH} = 2 \leftarrow 0$ H_2O overtone band region to achieve quantum state-resolved rovibrational excitation of the Ne–H_2O dimer. A second pulse from an ArF excimer laser (193 nm, 15 mJ) arrives after a delay time τ_1, which excites the H_2O substituent to a dissociative electronic state via the $A(^1B_1)$-$X(^1A_1)$ band enhanced by approximately two orders of magnitude for vibrationally excited H_2O and Ne–H_2O clusters.[41] Therefore, photolysis of any vibrationally excited H_2O containing clusters occurs selectively and rapidly on the dissociative $A(^1B_1)$ surface, with the resulting photoejected OH fragments probed by laser induced fluorescence (LIF) with a third pulse from the frequency doubled output of a DCM dye laser, detected with a 10 ns gated photomultiplier (PMT, 10 ns, Thorn EMI), captured by a box car integrator, digitized in a fast A/D converter, and stored for later analysis. This LIF laser in turn (~0.1-1 mJ) is tuned over the full OH ($A^2\Sigma \leftarrow X^2\Pi$) band to yield nascent rovibrational, spin orbit, and lambda doublet populations in $OH(^2\Pi_{1/2,3/2}; N; v = 0, 1)$.

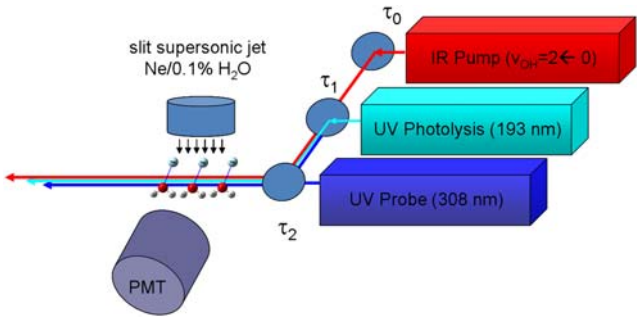

FIG. 1. Experimental schematic of the vibrationally mediated photolysis (VMP) slit jet spectrometer, with spatially overlapping IR pump, and UV photolysis and UV probe laser pulses along the long axis of a slit jet supersonic expansion. Vibrational overtone spectroscopy ($v_{OH} = 2 \leftarrow 0$) and predissociation dynamics of the clusters can be probed by tuning of the IR laser frequency and the pump-photolysis time delay, respectively (see text for details).

To further minimize background contributions from *non-vibrationally mediated* photolysis of H_2O clusters, the LIF probe laser is triggered at 5 Hz, with alternating signals subtracted in an every-other-pulse mode. The net result is a high background rejection method for identifying extremely weak rovibrational overtone transitions in H_2O containing cluster species, selectively leveraged by strong vibrationally enhanced 193 nm UV photolysis of H_2O in the overtone ($v_{OH} = 2$) manifold of states. As dissociation of the Ne–H_2O clusters energetically requires loss of the initially vibrationally excited quantum state of the H_2O subunit, this also provides an opportunity to probe evolution of the overtone excited cluster species in real time. Specifically, by varying the delay (τ_1) between infrared and photolysis pulses, one can thereby directly monitor population loss and thus quantum state-resolved vibrational predissociation dynamics in the Ne–H_2O cluster.

III. *AB INITIO*/QUANTUM CALCULATIONS

To make the most rigorous and direct comparison between the experiment and theory, we have performed fully converged bound state calculations of the lowest internal rotor energy levels on a high-level Ne–H_2O potential surface. As described previously,[21] the *ab initio* Ne–H_2O potential surface has been calculated by means of explicitly correlated coupled-cluster methods [CCSD(T)-f12b] implemented in the MOLPRO package[42] with the specially optimized, correlation consistent basis sets of Peterson *et al.* (VnZ-f12, n = 3, 4).[43] All energies have been corrected for basis set superposition error (BSSE) with the counterpoise (CP) correction method, whereby the individual Hartree-Fock reference, correlation and perturbative triples (T) energies have been individually extrapolated to the complete basis set (CBS) limit.[44,45] The main features of the Ne–H_2O PES have been investigated and discussed previously[8,32] and are reproduced by our PES. The global minimum geometry at E = –63.5 cm^{-1} corresponds to the Ne atom at R = 3.21 Å, θ = 73°, and ϕ = 0° with respect to the H_2O center of mass (with the C_2 axis of H_2O as the z axis and H atoms pointing downward), which compares well with earlier efforts.[8,32]

To obtain the bound states for ground state Ne–H_2O, we use the variational approach for van der Waals complexes which has been described previously,[23,46] with the Hamiltonian matrix diagonalized in a basis of angular and radial product functions. The energies of the rovibrational levels are converged to within 10^{-4} cm^{-1}, with bound states calculated for all values of J from 0 to 10. To compute the metastable Feshbach resonance energy levels corresponding to *excited* vibrational states of the H_2O monomer ($|02^+\rangle$, $|02^-\rangle$, $|11^+\rangle$), we use the same intermolecular potential, but with different

H_2O effective rotational constants A_v, B_v, and C_v chosen to reproduce the spectroscopically observed rigid rotor energies of the j_{kakc} = 1_{01} (B + C), 1_{11} (A + C), 1_{10} (A + B) rovibrational states in each vibrational manifold of H_2O. This should be entirely sufficient, as these lowest few rotational H_2O levels are the dominant components of the internal rotor states thermally populated in the Ne–H_2O complex.[47]

In order to obtain a complete *ab initio* prediction of the spectra, we use wave functions from the bound state calculations to compute line strengths for all allowed ΔJ = 0, ±1 transitions between the rovibrational states of the H_2O–Ne complex for J = 0–10 that accompany transitions of the H_2O monomer from its vibrational ground state $|00^+\rangle$ to the $|02^+\rangle$, $|02^-\rangle$, and $|11^+\rangle$ vibrationally excited states, where we utilize the local mode notation of Child and co-workers.[48,49] The formulae used to compute the line strengths have been taken from Ref. 22, where they have been explicitly derived. *Ab initio* overtone absorption spectra are then predicted based on assuming a Boltzmann rotational distribution (at some T_{rot}) of lower states, convoluting over a laser line width (Δν ≈ 0.20 cm^{-1}), and summing over all allowed transitions to upper states.

IV. RESULTS

A. Vibrationally mediated photolysis (VMP) spectroscopy (v_{OH} = 2 ← 0)

As described above, fully converged quantum dynamical calculations have been performed on the *ab initio* 3D potential surface for all bound internal rotor states in Ne–H_2O of *ortho*/*para* nuclear spin symmetry and e/f parity. Based on these eigenvalues and transition dipole matrix elements, fully *ab initio* spectral predictions for the experimental overtone band with sufficient intensity to be observed can be anticipated based on the following line of logic. (i) The lowest 1_{11} and 1_{10} excited rotor states of *para*- and *ortho*-H_2O are approximately A − C ≈ 18.6 cm^{-1} and A + C ≈ 37.19 cm^{-1} above their corresponding ground states, respectively. At a typical slit supersonic expansion temperature, therefore, the only appreciably populated internal rotor states of Ne–H_2O correlate asymptotically with *para* (0_{00}) and *ortho* (1_{01}) H_2O $|00^+\rangle$, with the *ortho* vs. *para* complexes favored by 3:1 nuclear spin statistics and unable to cool further. (ii) The v_{OH} = 2 stretch polyad in free H_2O can be accessed via three transitions from the ground state ($|02^-\rangle \leftarrow |00^+\rangle$: $|02^+\rangle \leftarrow |00^+\rangle$: $|11^+\rangle \leftarrow |00^+\rangle$) with a rapidly decreasing ratio of oscillator strengths (1.0:0.11:0.0065) that greatly favors internal rotor transitions built on $|02^+\rangle \leftarrow |00^+\rangle$ or $|02^-\rangle \leftarrow |00^+\rangle$ and eliminates $|11^+\rangle \leftarrow |00^+\rangle$ from further consideration. (iii) Although vibrational states in clusters can be remarkably metastable due to slow V → T energy transfer, internal rotor predissociation (R → T) is typically a fast process, fragmenting on the ps or shorter time scale. Therefore, only transitions to states rigorously bound with respect to internal rotor predissociation will be sufficiently long lived to be experimentally detected. For Ne–H_2O dissociation energies of D_0 = 31.67 cm^{-1} (*para*) and 34.66 cm^{-1} (*ortho*), this restricts consideration (with one exception, see Sec. V) to cluster states correlating asymptotically with the j_{kakc} = 0_{00}, 1_{01}, and 1_{11} (+37.19 cm^{-1}) H_2O free rotor. (iv) Finally, any monomer state with j > 0 will be split by anisotropy in the potential surface into j + 1 K projection states, where the internal rotor splittings in Ne–H_2O are sufficiently small [e.g., $E(\Pi_{1_{01}}) - E(\Sigma_{1_{01}}) \approx 5.2$ cm^{-1}] to be appreciably populated under typical supersonic jet conditions.

Based on this line of argument, one predicts *three* Ne–H_2O internal rotor bands built on *ortho*-H_2O (j_{kakc} = 1_{01}) to be observable in the 7210-7240 cm^{-1} spectral region. The two strongest bands will arise from the stronger $|02^-\rangle \leftarrow |00^+\rangle$ vibrational overtone transition out of the most populated (1_{01} *ortho*-H_2O) lower states, i.e., $|02^-\rangle\ \Sigma(0_{00}) \leftarrow |00^+\rangle\ \Sigma(1_{01})$, $|02^-\rangle\ \Sigma(0_{00}) \leftarrow |00^+\rangle\ \Pi(1_{01})$. Based on *ab initio* internal rotor energies for the ground state and experimental energies of the H_2O overtone states from the work of Tennyson *et al.*,[47] this predicts the two solid green arrow transitions shown to the left in Fig. 2. There will also be an additional pair of Π ← Σ, Π ← Π and Σ ← Σ, Σ ← Π bands built on the 9.2-fold weaker $|02^+\rangle \leftarrow |00^+\rangle$ overtone transition out of the (*ortho*-H_2O) ground state $\Pi^{e/f}(1_{01})$ and $\Sigma^e(1_{01})$ internal rotor levels. However, if one considers the additional Boltzmann penalty (6.5× weaker) for the 5.2 cm^{-1} Π–Σ splitting in the lower state, plus the 9.2× loss ($|02^+\rangle \leftarrow |00^+\rangle$ vs. $|02^-\rangle \leftarrow |00^+\rangle$) in vibrational oscillator strength, the only observable feature will likely be due to accumulated intensity in overlapping (f ← e) Q-branch transitions arising from the perpendicular Π ← Σ band [i.e., $|02^+\rangle\ \Pi^{e/f}(1_{10}) \leftarrow |00^+\rangle\ \Sigma^e(1_{01})$]. Relying as before on *ab initio* Ne–H_2O internal rotor eigenvalues and literature

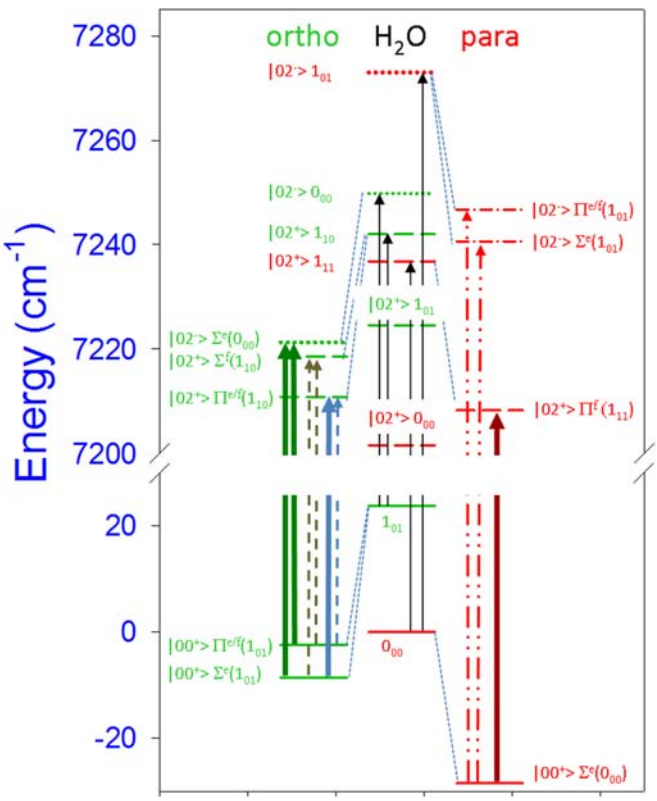

FIG. 2. Allowed transitions in *ortho*- and *para*-Ne–H_2O. H_2O is treated as a hindered asymmetric rotor with states labeled according to H_2O overtone excitation ($|02^-\rangle$ or $|02^+\rangle$), H_2O rotational state (j_{kakc}), and projection (Σ, Π) along the body-fixed intermolecular cluster axis. Vertical lines correspond to observed (solid) and unobserved (dashed) transitions under the current sensitivity conditions.

values for the monomer overtone levels,[47] one therefore arrives at four additional fully *ab initio* predictions for *ortho*-Ne–H_2O complexes marked in the left-hand side of Fig. 2 by the one solid (blue) and three dashed arrows (olive and blue) for the stronger and weaker transitions, respectively.

Following a similar reasoning, there will also be formation of $\Sigma^e(0_{00})$ *para*-Ne–H_2O clusters built on the corresponding $j_{kakc} = 0_{00}$ internal rotor state of the H_2O monomer. This lower state yields spectral predictions shifted to the blue (7260 cm^{-1}–7280 cm^{-1}), as illustrated in the right-hand side of Fig. 2. Specifically for excitation in the $|02^-\rangle \leftarrow |00^+\rangle$ vibrational manifold, one would predict two strong internal rotor bands out of $\Sigma^e(0_{00})$ accessing the $\Pi^{e/f}(1_{01})$ and $\Sigma^e(1_{01})$ upper states, weakly split by anisotropy in the Ne–H_2O intermolecular potential and marked in Fig. 2 as dashed lines (red). Corresponding *para* signals in the $|02^+\rangle \leftarrow |00^+\rangle$ vibrational manifold might be anticipated to be very weak, as B-type transitions out of the lowest 0_{00} (*para*) internal rotor states will only access transitions correlating with the 1_{11} (*para*) monomer, which occur at energies substantially higher than the lowest $|02^+\rangle 0_{00}$ (*para*) asymptotic channels and thus can in principle rapidly predissociate. Surprisingly, this turns out not to be the case due to the absence of a final state manifold of the correct total parity, which as we shall see (*vide infra*) is made experimentally evident for one (and only one) branch in the *para* manifold.

These simple *ortho* and *para* predictions invite detailed comparison with the experimental VMP spectra. Sample IR-UV-UV spectral data over the *ortho*-Ne–H_2O $v_{OH} = 2$ overtone region (7210-7240 cm^{-1}) are shown in Fig. 3, obtained by (i) tuning the infrared laser frequency, (ii) photolyzing at 193 nm after τ = 150 ns, and (iii) monitoring fluorescence on the $Q_{11}(N = 8)$ OH transition at 309.24 nm. The long time delay between infrared and photolysis beams ensures that vibrational predissociation of the Ne–H_2O cluster species is complete before OH detection. Each feature in the spectrum is rigorously confirmed to be a result of vibrationally excited molecules or clusters in the supersonic jet by IR on/off background subtraction. As expected, the spectra are dominated by a few strong overtone transitions in free H_2O. However, additional contributions from Ne–H_2O clusters are clearly evident as multiple P/R and unresolved Q-branch features in the spectrum, with band origins in remarkable agreement with the "first principles" *ab initio* theoretical predictions made in Fig. 2 and denoted by solid green, blue, and red arrows.

Quantitatively, the strongest predicted Ne–H_2O band occurs at 7229.63 cm^{-1} and exhibits a clear $\Sigma \leftarrow \Sigma$ structure, which, due to the partially rotationally resolved P/R branch structure and absence of a Q branch, can be unambiguously assigned to the $|02^-\rangle\ \Sigma(0_{00}) \leftarrow |00^+\rangle\ \Sigma(1_{01})$ internal rotor transition in *ortho*-Ne–H_2O. This band is slightly blue-shifted from the more intense $|02^-\rangle\ 0_{00} \leftarrow |00^+\rangle\ 1_{01}$ overtone line in H_2O, consistent with the theoretical prediction of greater Ne-induced stabilization for the ground $\Sigma(1_{01})$ vs. first excited $\Pi(1_{01})$ internal rotor components correlating with 1_{01} H_2O. From the *ab initio* energy level patterns in Fig. 2, a slightly

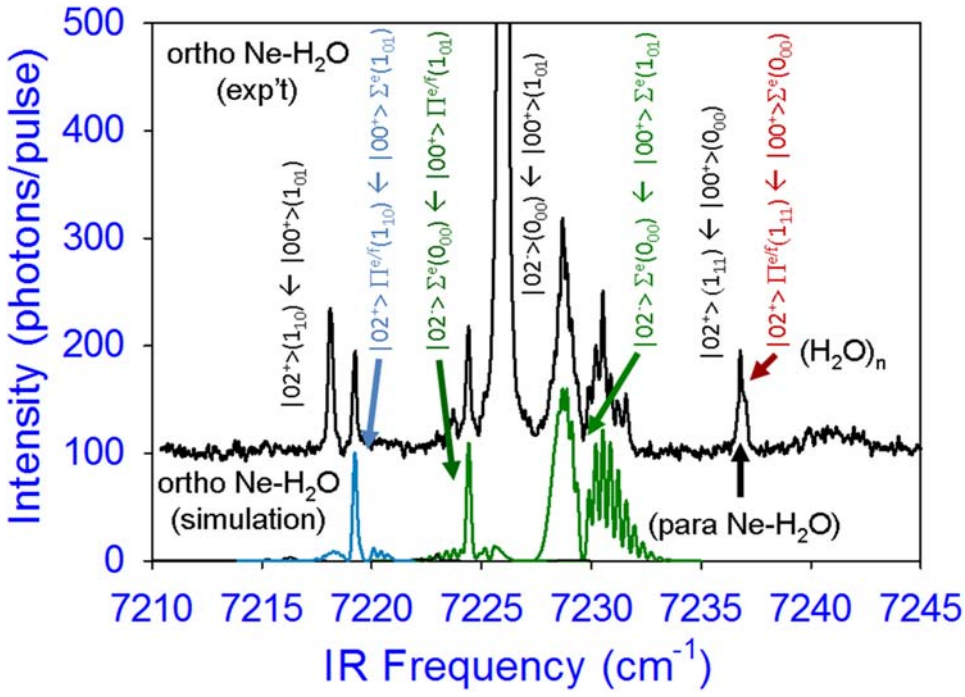

FIG. 3. Comparison of experimental and fully *ab initio* spectral predictions for vibrationally mediated photolysis (VMP) of *ortho*-Ne–H_2O clusters. All predictions are based on (i) *ab initio* calculated energy levels and intensities, (ii) Boltzmann internal rotor and rotational distributions at T_{rot} = 4 K, (iii) 9.2:1 integrated intensity ratio for the $|02^-\rangle \leftarrow |00^+\rangle$ and $|02^+\rangle \leftarrow |00^+\rangle$ overtone bands, and (iv) IR pump laser linewidth of $\Delta\nu = 0.20$ cm^{-1}. Experimental (black) and theoretical (blue and green) $v_{OH} = 2$ overtone spectra are shown for *ortho*-H_2O and Ne–H_2O clusters, where the colors of the rotational band contours for the cluster species match the arrows in Fig. 2. Note also the accurate prediction of strong Q-branch signals (dark red) at 7237.00 cm^{-1} due to the *para*-Ne–H_2O $|02^+\rangle\Pi^f(1_{11}) \leftarrow |00^+\rangle\Sigma^e(0_{00})$ band, where the upper f state is parity forbidden from predissociating via internal rotation to the $|02^+\rangle\Sigma^e(0_{00})$ state (see text and Fig. 7 for details). The spectral feature near 7241.2 cm^{-1} corresponds to a predissociatively broadened $(H_2O)_n$ cluster overtone band in the $v_{OH} = 2$ polyad with $n > 2$.

weaker $\Sigma \leftarrow \Pi$ band is also predicted and indeed observed at 7224.40 cm^{-1}, which arises from transitions out of the corresponding first excited $\Pi(1_{01})$ internal rotor manifold. Due to finite IR pump laser resolution ($\Delta\nu \approx 0.20$ cm^{-1}), the many overlapping transitions in the Q branch form by far the most prominent feature, but the weaker P branch structure is also evident to the red, with the corresponding R branch structure apparent only as a shoulder on the strong $|02^-\rangle\, 0_{00} \leftarrow |00^+\rangle\, 1_{01}$ H_2O overtone pedestal. Note that since both transitions access the same $|02^-\rangle\, \Sigma(0_{00})$ upper state, the spacing of these $\Sigma \leftarrow \Sigma$ and $\Sigma \leftarrow \Pi$ bands provides a direct estimate ($\Delta\nu \approx 5.2$ cm^{-1}) for the Σ–Π internal rotor splitting in the ground vibrational manifold. As evident from Fig. 2, these are the only infrared active *ortho*-Ne–H_2O bands predicted from transitions built on the $|02^-\rangle \leftarrow |00^+\rangle$ H_2O monomer vibration.

Also as predicted, a third band is evident near 7219.25 cm^{-1} and, again based on energy and intensity predictions from the *ab initio*/quantum calculations, can be unambiguously assigned to $\Pi(1_{10}) \leftarrow \Sigma(1_{01})$ transitions in the substantially weaker $|02^+\rangle \leftarrow |00^+\rangle$ overtone manifold. Note that the perpendicular structure for a Π–Σ band yields a strong Q branch of nearly comparable intensity to the $\Sigma \leftarrow \Pi$ internal rotor band mentioned above. Since all three of these bands originate from states correlating with *ortho* 1_{01} H_2O, this suggests that the 9.2-fold decrease in $|02^+\rangle \leftarrow |00^+\rangle$ vs. $|02^-\rangle \leftarrow |00^+\rangle$ overtone line strength is very roughly matched by the exp(−ΔE/kT) Boltzmann factor for populating the first excited $\Pi(1_{01})$ vs. ground state $\Sigma(1_{01})$ internal rotor level. As noted above, this Σ–Π internal rotor splitting is experimentally observed to be $\Delta E = 5.2$ cm^{-1}, which would suggest a rotational temperature of $T_{rot} \approx 4$ K. It is worth noting that this rotational temperature is 2-3 times colder than typically observed ($T_{rot} \approx 10$ K) in our slit jet supersonic expansions but, as shown in Fig. 3, proves to be consistent with detailed rotational modeling of the $|02^-\rangle$ $\Sigma(0_{00}) \leftarrow |00^+\rangle$ $\Sigma(1_{01})$ band.

Of particular dynamical interest, the *only para* internal rotor band of Ne–H_2O is evident in Fig. 3 near 7237.00 cm^{-1}, specifically as the unresolved Q-branch structure on the blue side of the $|02^+\rangle(1_{11}) \leftarrow |00^+\rangle(0_{00})$ overtone transition in the H_2O monomer. From the *ab initio* bound state calculations, this is in excellent agreement with predictions for the $\Pi^{e/f}(1_{11}) \leftarrow \Sigma^e(0_{00})$ internal rotor band of the *para*-H_2O monomer. What makes this initially quite surprising is that this transition is already at an energy 6-8 cm^{-1} *in excess* of the Ne + H_2O $|02^+\rangle\, 0_{00}$ dissociation limit. Unlike predissociation via vibrational to translational (V-T) energy transfer, which can be extremely slow by virtue of frequency mismatch, rotational to translational (R-T) predissociation is typically extremely rapid, occurring on the time scale of a few rotational periods. Therefore, the clear observation of strong VMP signals in this region speaks to a novel source of dynamical metastability in the upper $\Pi^f(1_{10})$ internal rotor manifold, which will be discussed in more detail in Sec. V C.

B. Real time vibrational predissociation dynamics

With the internal rotor transitions in Ne–H_2O spectroscopically assigned, we can now directly monitor the vibrational mediated decay of Ne–$H_2O \rightarrow H_2O$ + Ne in real time using time-resolved pump-probe methods. The simple reason why this is even observable in our experiment is that the probability to produce a given rovibrational, spin orbit, and lambda doublet state of OH by the UV photolysis laser depends sensitively on the rovibrational state of the H_2O achieved by predissociation. Fortunately, the dynamics of quantum state selective vibrationally mediated photolysis of H_2O has been extensively studied in a series of seminal papers by several groups. Of particular relevance are the pioneering experimental studies by Andresen and co-workers,[50–53] for which UV photolysis of H_2O in the lowest *para* 0_{00} or *ortho* 1_{01} states was found to fragment into rotationally *cold* OH products.[50–53] With a full quantum treatment developed by Schinke and co-workers,[52–54] the simple semiclassical picture is that the H atom recoils predominantly against the O atom and therefore exerts only a small torque on the resulting OH photofragment. Instead, the photolysis dynamics is sudden, with final OH rotational distributions approximately estimated via the Franck Condon projection of the H_2O wavefunction onto free rotor states of the asymptotic H + OH products.

Schinke's treatment indicates that photolysis of the nodeless ground state HOH bending wavefunction results in low OH rotational excitation, but with a distribution that heats up dramatically for $v_2 > 0$. Thus, predissociated Ne–H_2O clusters with significant HOH bending excitation can be sensitively and selectively detected by probing OH in *high* rotational states. Furthermore, from simple energy/quantum gap law concepts developed by Ewing,[35] intramolecular vibrational relaxation into the Ne–H_2O cluster is anticipated to strongly minimize energy transfer into translational degrees of freedom and the number of vibrational quanta exchanged. Thus, loss of the initial $|02^+\rangle$ or $|02^-\rangle$ overtone state would be expected to occur predominantly via small quantum and energy gap processes such as $\Delta v_{OH} = -1$ ($\Delta E \approx 3500$ cm^{-1}) which could energetically and near-resonantly access states with two quanta in the HOH bend, i.e., $|01^\pm\rangle|v_{bend} = 2\rangle$. Combining these two dynamical effects, one predicts that the *appearance* of high OH rotational states as a function of time delay between IR pump/UV photolysis lasers will elucidate the real-time vibrational predissociation *disappearance* of the excited Ne–H_2O clusters.

By way of an example, Fig. 4 displays a sample time trace for IR pumping of the Ne–H_2O clusters on the $|02^+\rangle\, \Pi(1_{10}) \leftarrow |00^+\rangle\, \Sigma(1_{01})$ internal rotor band, while monitoring appearance of highly rotationally excited OH state photofragments on the $Q_{11}(N = 8)$ transition. Since photolysis of H_2O $|02^\pm\rangle$ in the absence of Ne generates much colder OH species (as shown explicitly in Sec. V A), the exponential rise in the OH signal with increasing time delay (τ_1) of the UV photolysis beam reflects the time-dependent increase in predissociated H_2O products. More quantitatively, these traces can be fit to a convolution for single exponential rise in the dissociated Ne–H_2O cluster fraction $(1-e^{-(\frac{t}{\tau})})$ over a Gaussian instrument response function [$IRF(t) = e^{-(\frac{t}{\sigma})^2}$] to yield

$$S(t) = \frac{B}{2} e^{-(\frac{t-t_0}{\tau})} e^{\frac{\sigma^2}{4\tau^2}} \left(1 + erf\left(\frac{t-t_0}{\sigma} - \frac{\sigma}{2\tau}\right)\right) + \frac{B}{2}\left(1 + erf\left(\frac{t-t_0}{\sigma}\right)\right), \quad (1)$$

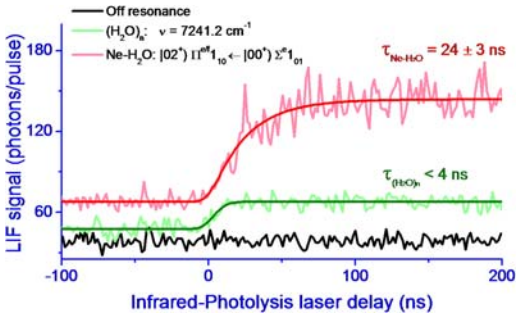

FIG. 4. Real-time vibrational predissociation dynamics in metastable Ne–H_2O clusters (in red), obtained by (i) pulsed IR overtone excitation to a metastable cluster state, (ii) 193 nm UV photolysis after a time delay τ, and (iii) LIF detection of OH (N = 8) fragments. The sensitivity to vibrational predissociation dynamics arises from a propensity for formation of highly rotationally excited OH exclusively via photolysis of $|v_2 \geq 1\rangle$ H_2O states, which in turn are generated in Ne–H_2O by near-resonant intramolecular energy transfer of a single quantum of OH stretch. Also shown (in green) is a sample vibrational predissociation data for IR laser excitation of an unassigned $(H_2O)_{n>2}$ transition, demonstrating both an instrument limited rise (<4 ns) and a reduced propensity for yielding high rotational states of OH. Also shown are background signals (black) corresponding to non-vibrationally mediated photolysis of H_2O in the supersonic jet obtained by tuning the IR laser off resonance for any cluster absorption.

where B is the overall signal amplitude and t_0 is the arrival time of the IR pulse. The IRF response can be independently measured by cross correlation between IR pump and UV photolysis lasers in parallel studies of the H_2O monomer, for which appearance of OH is essentially instantaneous, with the observed results [σ = 8(2) ns] entirely limited by finite laser pulse duration. In clear contrast, fits to OH appearance from $|02^+\rangle$ $\Pi(1_{10})$ vibrationally excited Ne–H_2O clusters reveal a much longer single exponential rise, well in excess of the instrument response function and consistent with a predissociation lifetime of τ_{predis} = 24(3) ns, where the number in parentheses represents a 1σ uncertainty in the result. Note that alternating laser pulse subtraction methods are intentionally not used to collect the data in Fig. 4, which therefore results in a finite background due to weak, non-resonant UV photolysis of H_2O in the chamber and thus a baseline offset independent of the IR pump frequency. As expected, the background data trace (black) in Fig. 4 illustrates an insensitivity in the offset to both (i) pump-photolysis delay and (ii) infrared laser detuning from all water monomer and cluster transitions.

Also shown in Fig. 4 is a sample time delay trace (green) for the infrared laser tuned to one of the several rotationally unstructured and unassigned $(H_2O)_n$ water cluster bands (with n ≥ 2) evident throughout the spectrum. Note that these pump-probe signals also show a clear time-dependent *increase* in the OH concentration, indicating that vibrational excitation even in water dimers, trimers, or larger clusters results in an increase of high OH rotational state population. However, the rise times are now clearly faster than the instrument response function, with least squares fits to Eq. (1) placing an upper limit on $(H_2O)_{n\geq 2}$ cluster predissociation lifetimes of ≤4 ns. Indeed, the lack of observable rotational structure on these $(H_2O)_{n\geq 2}$ bands is at least consistent with this upper limit and would suggest τ_{predis} < 100 ps for the time scale of such predissociation events. However, it is worth noting that predissociation lifetimes even on the ns time scale would be consistent with previous VMP spectroscopic studies of $(H_2O)_2$ in the 7193 cm^{-1} $v_{OH} = 2 \leftarrow 0$ region, for which the rotational structure could be clearly resolved, successfully analyzed, and assigned to either (i) single quantum excitation of both free and bound OH stretches $(|1\rangle_{free}|1\rangle_{bound})$ or (ii) direct excitation of the symmetric OH stretch overtone in the acceptor species $(|02^+\rangle_{acceptor})$.[17,41]

V. DISCUSSION

A. OH (N) photofragment product state distributions

The triple resonance laser capabilities permit these VMP spectroscopy methods to be extended in several directions. As one example, for infrared excitation to a given Ne–H_2O internal rotor state, followed by 193 nm photolysis after a sufficiently long time delay (τ = 150 ns) to ensure complete predissociation of the cluster, one can explore product state distributions of the photolytically generated OH product as a function of the final rotational, spin orbit, and lambda doublet state. This is of particular relevance to the present study, as the VMP spectra shown in Fig. 5 have been obtained by probing high rotational OH(N = 8) states in order to selectively enhance contributions from vibrationally mediated cluster vs. H_2O monomer photolysis. By scanning over the nascent OH photoproduct as a function of the UV probe laser frequency, this assumption can be tested quantitatively. Specifically, Fig. 5 displays the average energy in OH rotation, sorted by the spin orbit and lambda doublet state, obtained from laser excitation at the maximum (7230.5 cm^{-1}) of the $|02^-\rangle$ $\Sigma(0_{00}) \leftarrow |00^+\rangle\Sigma(1_{01})$ R-branch (J = 3 ← 2). Also shown for comparison are the average rotational energies similarly obtained via vibrationally mediated photolysis of H_2O monomers (i.e., in the *absence* of the Ne atom) for the same $|02^-\rangle$ $0_{00} \leftarrow |00^+\rangle$ 1_{01} transition. As predicted, the data indicate that the degree of OH(N) rotational excitation is very strongly enhanced by photolysis events from vibrationally mediated cluster vs. monomer species, by factors between 5:1 and 20:1 as a function of the final spin orbit state.

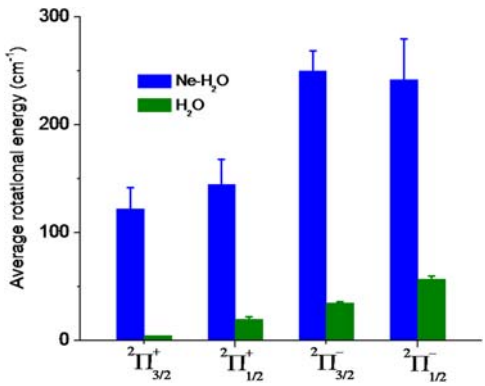

FIG. 5. Average rotational energy observed in each of the OH rotational, spin orbit, and lambda doublet sub-levels after (i) pulsed infrared excitation of *ortho*-Ne–H_2O $[|02^-\rangle\, \Sigma^e(0_{00}) \leftarrow |00^+\rangle\, \Sigma^e(1_{01})]$, (ii) 150 ns delay to permit complete vibrational predissociation to Ne + H_2O fragments, and (iii) UV photolysis at 193 nm. Note the 5- to 20-fold higher degree of OH rotational excitation achieved for vibrationally mediated photolysis of Ne–H_2O than for *ortho*-H_2O monomer after excitation to the same asymptotic rotor state.

Such dramatic differences in these rotational distributions suggest that a robust, common mechanism must be controlling the predissociation dynamics. Though further theoretical efforts modeling the overtone cluster photolysis dynamics may be necessary for confirmation, we offer the following simple physical picture. As mentioned previously in Sec. IV B, the density of rovibrational states for asymptotically dissociated Ne + H_2O is extremely sparse, and dynamical "exponential gap law" propensities[35] in unimolecular fragmentation events for minimizing energy release into translation are very high. Thus, the most probable pathway would be predissociation via near-resonant unimolecular energy transfer to form rotationally excited $\{|01^+\rangle; |v_2 = 2\rangle\}$ ($\Delta E = -455$ cm^{-1}) or $\{|01^-\rangle; |v_2 = 2\rangle\}$ ($\Delta E = -359$ cm^{-1}) states of the asymptotic H_2O monomer, releasing sufficient energy to readily dissociate the cluster ($D_0 \approx 32$-35 cm^{-1}). The critical point is that H_2O ejected from the cluster has both (i) one quantum of OH stretch excitation and (ii) multiple quanta of the HOH bend, which is optimally suited to the current VMP detection scheme. Specifically, $v_{OH} = 1$ excitation strongly facilitates the 193 nm photolysis channel to form H + OH, as demonstrated by the Andresen and Crim groups,[50–53] while photolysis of the HO–H bond with two quanta of bending excitation leads to high rotational states in the nascent OH, as established by Schinke and co-workers.[51–55] The net result is a synergistic enhancement in both photolysis sensitivity and probe selectivity for the vibrationally mediated predissociation event.

B. *Para-* vs. *ortho*-Ne–H_2O spectra and nuclear spin dependent predissociation dynamics

The corresponding experimental and theoretical predictions for Ne–H_2O transitions in the *para*-H_2O manifold are presented in Fig. 6, with identical intensity scaling as described for the *ortho*-H_2O manifold transitions in Fig. 3. Simply summarizing, we see no evidence at current sensitivity levels for the VMP spectra of any Ne–H_2O clusters excited in the corresponding *para*-H_2O manifold. It is important to note that

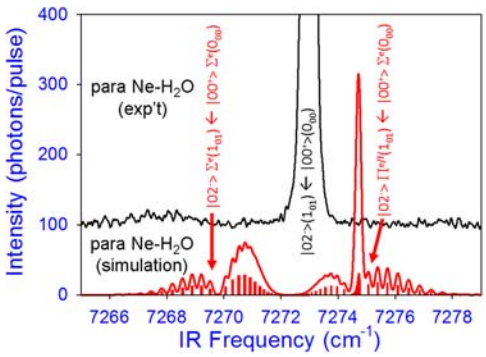

FIG. 6. Comparison of experimental and fully *ab initio* spectral predictions for vibrationally mediated photolysis (VMP) of *para*-Ne–H_2O clusters. All predictions are based on (i) *ab initio* calculated energy levels and intensities, (ii) Boltzmann internal rotor and rotational distributions at $T_{rot} = 4$ K, (iii) 9.2:1 integrated intensity ratio for the $|02^-\rangle \leftarrow |00^+\rangle$ and $|02^+\rangle \leftarrow |00^+\rangle$ overtone bands, and (iv) IR pump laser linewidth of $\Delta\nu = 0.20$ cm^{-1}. Comparison of the experiment with *ab initio* theory (red) for *para*-Ne–H_2O clusters, with the same relative intensity scaling as in Fig. 3. Note the *absence* of VMP signals from *para*-Ne–H_2O clusters in this spectral region despite predictions of particularly strong overlapping Q-branch signals near 7274.5 cm^{-1} with S/N > 50.

this is despite highly accurate predictions for the corresponding *ortho*-Ne–H_2O absorption band origins ($\Delta E \approx 0.07$ cm^{-1} –0.60 cm^{-1}) and predicted Q-branch intensities 30-40 times in excess of the signal-to-noise limit. It is worth stressing, however, that the experimental VMP data represent "action" spectra, with intensities proportional not only to (i) the initial overtone absorption step but also to (ii) the explicit mechanism for vibrational predissociation and (iii) UV photolysis efficiency to form the particular probe quantum state. So, more accurately stated, the efficiency for OH(N = 8) generation from *para*-Ne–H_2O must be lower than that of *ortho*-Ne–H_2O by at least 30-40 fold. Predissociation and photolysis bond fission dynamics obviously cannot be influenced, at least directly, by the weak coupling of nuclear spins between the two identical H atoms. The obvious question, therefore, is what is the mechanism for such strongly contrasting *ortho*- vs. *para*-Ne–H_2O behavior in the spectra.

The *ab initio* theoretical predictions offer an elegantly simple physical reason for the dynamical differences between the *ortho*- and *para*-Ne–H_2O manifolds. Specifically, Fig. 7 reiterates all the relevant *ortho*-Ne–H_2O (left), *para*-Ne–H_2O (right), and H_2O monomer (center) energy levels, with alternating red vs. green color coding for *para* vs. *ortho* states. The energetics in Fig. 7 immediately identify the obvious mechanism: each of the three *ortho*-Ne–H_2O nuclear spin states accessed by overtone pumping lie *below* (and thus *the ortho clusters are energetically stable* with respect to the formation of) the nearby $|02^+\rangle$ 1_{01} asymptotic state of *ortho*-H_2O. As a result, energy conservation requires that predissociation to form Ne + H_2O *must* first require intramolecular vibrational energy transfer out of the initial $v_{OH} = 2$ overtone state, the most resonant downhill pathway for which would be into the $\{|01^\pm\rangle; v_2 = 2\}$ manifolds. Once again, populations in these excited OH stretching and HOH bending states in the monomer enhance both (i) 193 nm UV cross sections for photolysis and (ii) H_2O photofragmentation to form highly rotationally excited OH(N). Consequently, $v_{OH} = 2 \leftarrow 0$ overtone absorption events in the *ortho*-Ne–H_2O manifold are energetically forced into a pathway that facilitates efficient formation of OH(N = 8) and is thus readily detected as the VMP signal.

For the *para*-Ne–H_2O manifold, on the other hand, Fig. 7 shows that the two states accessed $\{|02^-\rangle\ \Pi^{e/f}(1_{01})$ and $\{|02^-\rangle\ \Sigma^e(1_{01})\}$ lie *above and therefore are energetically accessible* to either asymptotic $|02^+\rangle$ 0_{00} or $|02^+\rangle$ 1_{11} states of the correct *para* nuclear spin symmetry. Intracluster energy transfer from the $|02^-\rangle \rightarrow |02^+\rangle$ manifolds is thus anticipated to be facile, as these two states (i) are nearly resonant in energy ($\Delta E \approx 50$ cm^{-1}) and (ii) require only a collisional rephasing of the local mode OH stretch motions by the Ne atom. Indeed, collisional energy transfer in the corresponding $v_{OH} = 1$ polyad has been shown to be a nearly gas-kinetic process by Moore and co-workers.[56] However, 193 nm photolysis of the resulting asymptotic $|02^+\rangle$ H_2O state does not efficiently form high N states of the OH photofragment (see Fig. 5). Thus, $|02^-\rangle \leftarrow |00^+\rangle$ overtone absorption events in jet-cooled *para*-Ne–H_2O clusters will not enhance [OH(N = 8)] concentrations sampled by the UV probe laser, to which the triple resonance VMP spectra are therefore optically insensitive.

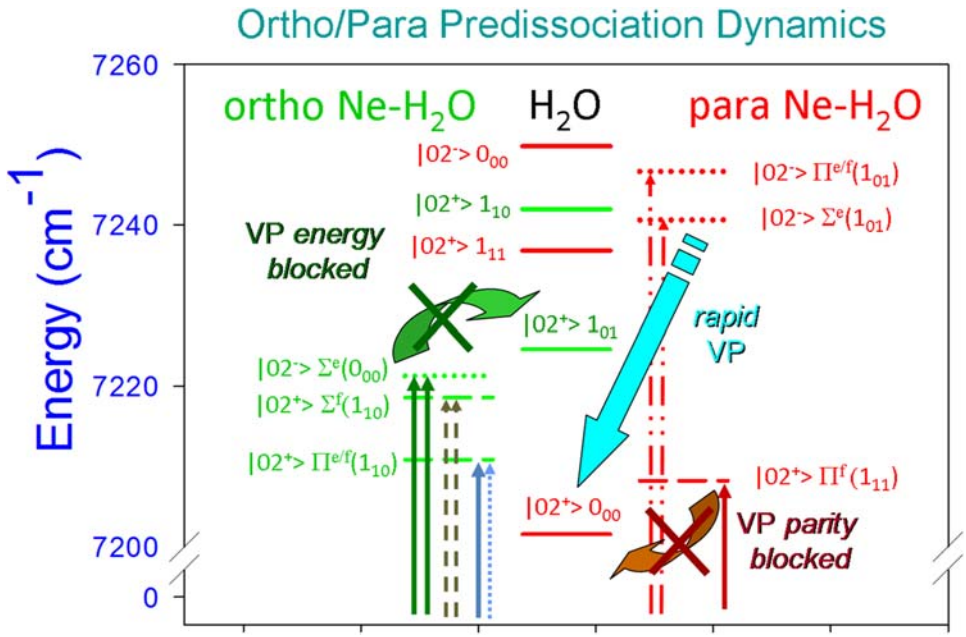

FIG. 7. Expanded *ab initio* energy level diagram for $v_{OH} = 2 \leftarrow 0$ excited H_2O and Ne–H_2O clusters. The *ab initio* relative energy ordering of the states provides an elegantly simple physical picture for the presence of both (i) *ortho* vs. *para* nuclear spin symmetry and (ii) e/f parity-dependent predissociation dynamics experimentally observed in the Ne–H_2O VMP spectra. Simply summarizing, (i) the optically bright *ortho*-Ne–H_2O states (VP *energy blocked*, dark green) are energetically too low to access the only *ortho*-H_2O asymptotic channel ($|02^+\rangle 1_{01}$), (ii) the corresponding *para*-Ne–H_2O states (*rapid* VP, light blue) lie conveniently above a near-resonant *para*-H_2O asymptotic channel ($|02^+\rangle 0_{00}$), while the f-parity component of the *para*-Ne–H_2O $|02^+\rangle\ \Pi^{e/f}(1_{11})$ manifold (VP *parity blocked*, dark red) has no matching f-parity component in the asymptotic $|02^+\rangle\ 0_{00}$ state into which predissociation can occur (see text for details).

Additional confirmation of this very simple dynamical picture for *ortho-para* specificity can be obtained from parallel investigations of *para*-Ar–H_2O, which has also been studied by similar VMP methods in the $|02^-\rangle$ manifold. In contrast to the complete absence of signals from *para*-Ne–H_2O, excitation of the analogous upper states for *para*-Ar–H_2O yields *strong* VMP signals on *both* the $|02^-\rangle\ \Pi^{e/f}(1_{01}) \leftarrow |00^+\rangle\ \Sigma^e(0_{00})$ and $|02^-\rangle\ \Sigma^e(1_{01}) \leftarrow |00^+\rangle\ \Sigma^e(0_{00})$ bands. The reason for such apparently contrasting behavior follows immediately from the arguments presented above. The binding energy of Ar–H_2O ($D_0 \approx 100\ cm^{-1}$) is now $\approx 65\ cm^{-1}$ stronger than for Ne–H_2O, which is sufficient to bring the $|02^-\rangle\ \Pi^{e/f}(1_{01})$ and $|02^-\rangle\ \Sigma^e(1_{01})$ states in *para*-Ar–H_2O *energetically below* the asymptotically free $|02^+\rangle\ 0_{00}$ state of *para*-H_2O. Hence, near-resonant vibrational predissociation to $|02^+\rangle\ 0_{00}$ of free H_2O becomes *energetically inaccessible*. As argued previously for *ortho*-Ne–H_2O, *para*-Ar–H_2O therefore must predissociate via the near-resonant $\Delta v_{OH} = -1$, $\Delta v_2 = +2$ intramolecular vibrational transfer into the $\{|01^{\pm}\rangle;\ v_2 = 2\}$ manifold, which in turn photolyzes readily to yield strong signals from OH(N = 8). As summarized in Table I, the predissociation rates in these *para*-Ar–H_2O complexes have slowed down to the

TABLE I. Summary of assigned Ne–H_2O transitions (cm^{-1}) investigated via $v_{OH} = 2 \leftarrow 0$ overtone vibrationally mediated photolysis (VMP) spectroscopy and time-resolved vibrational predissociation (ns) methods, with previously studied Ar–H_2O [and unassigned $(H_2O)_{n>2}$ bands] for comparison. Note the much longer Ar–H_2O vs Ne–H_2O predissociation lifetimes, as opposed to the laser pulse width limited ($\tau_{IR\ pump}$, $\tau_{UV\ photolysis} \approx 4$ ns) bands observed for $(H_2O)_{n>2}$.

Species	Upper state	Lower state	Observed frequency	*Ab initio* frequency	Intensity (arb units)	$\tau_{prediss}$ (ns)
Ne–H_2O	Ortho $\|02^+\rangle\Pi^{e/f}(1_{10})$	Ortho $\|00^+\rangle\ \Sigma^e(1_{01})$	7219.2	7219.0	27	24(3)
Ne–H_2O	Ortho $\|02^-\rangle\ \Sigma^e(0_{00})$	Ortho $\|00^+\rangle\Pi^{e/f}(1_{01})$	7224.1	7224.2	43	18(2)
Ne–H_2O	Ortho $\|02^-\rangle\ \Sigma^e(0_{00})$	Ortho $\|00^+\rangle\ \Sigma^e(1_{01})$	7229.6	7229.7	309	15(2)
Ne–H_2O	Para $\|02^+\rangle\ \Pi^f(1_{11})$	Para $\|00^+\rangle\ \Sigma^e(0_{00})$	7237.0	7237.0	309	19(3)
Ar–H_2O	Ortho $\|02^-\rangle\ \Sigma^e(0_{00})$	Ortho $\|00^+\rangle\Pi^{e/f}(1_{01})$	7218.5			25(1)
Ar–H_2O	Ortho $\|02^-\rangle\ \Sigma^e(0_{00})$	Ortho $\|00^+\rangle\ \Sigma^e(1_{01})$	7230.7			26(1)
Ar–H_2O	Para $\|02^-\rangle\ \Pi^{e/f}(1_{01})$	Para $\|00^+\rangle\ \Sigma^e(0_{00})$	7275.2			52(2)
Ar–H_2O	Para $\|02^-\rangle\ \Sigma^e(1_{01})$	Para $\|00^+\rangle\ \Sigma^e(0_{00})$	7264.8			105(8)
$(H_2O)_{n>2}$			7241.2		58	4(4)
$(H_2O)_{n>2}$			7249.7		79	3(3)

50-100 ns time scale, easily long enough to measure in real time and, indeed, even an additional 2-4× longer than observed for *ortho*-Ar–H_2O.

In closing this section, it is worth stressing that in previous studies we were also not able to see *para*-H_2 complexes with either *ortho*- or *para*-H_2O.[22,23] We rationalized this by noting that the binding energy of *para*-H_2(j = 0) with H_2O was dramatically smaller than for *ortho*-H_2(j = 1) due to the inability of a spherical (j = 0) H_2 wave function to align optimally with respect to the H_2O target in the body-fixed frame. As a result, any *para*-H_2 complexes formed with H_2O will be thermodynamically displaced by the more strongly binding *ortho*-H_2 in the early regions of the supersonic slit jet expansion. We note, however, that we have successfully detected complexes of *ortho*-H_2 with *both ortho*- and *para*-H_2O, which suggests that the Ne–H_2O complex is stably formed with both *ortho*- and *para*-H_2O subunits. Thus, the lack of any *para*-H_2O signals once again can be attributed to an *absence* of rapid internal rotor predissociation dynamics in the corresponding Ne–H_2O cluster and is thus entirely consistent with the above mechanism.

C. Parity dependent metastability and predissociation dynamics in Ne–H_2O

As a parting comment, we briefly return to the *ab initio* energy level and spectral predictions in Figs. 2 and 7 in order to explain the one exception to the absence of any *para*-Ne–H_2O contributions to the VMP spectra. In the absence of external fields, the true parity operator (i.e., inversion of all coordinates through the origin) commutes with the total Hamiltonian. Therefore any eigenfunction of H can be rigorously labeled by its ± parity eigenvalue or, since total J is also a good quantum number, by the spectroscopic parity labels *e* or *f* corresponding to states of $(-1)^J$ or $(-1)^{J+1}$ true parity, respectively. What makes this of particular dynamical interest in *para*-Ne–H_2O is that *both* the *e* and *f* parity $\Pi^{e/f}(1_{11})$ internal rotor states are ≈37 cm^{-1} above the $\Sigma^e(0_{00})$ ground state manifold, i.e., in excess of the *para* nuclear spin symmetry-dependent dissociation energy, D_0 = 31.67 cm^{-1}. As a result, we argued correctly that the *e*-parity $\Pi(1_{11})$ states were therefore *dynamically unbound*, would relax via internal rotor predissociation to the $\Sigma^e(0_{00})$ manifold, and rapidly dissociate. However, this is *not true* for the corresponding *f*-parity component of the $\Pi(1_{11})$ manifold, which for any parity-conserving collision Hamiltonian must have exactly vanishing matrix elements for coupling with any *e*-parity manifold such as $\Sigma^e(0_{00})$. As a result, the $\Pi^f(1_{11})$ manifold represents a novel set of *energetically unbound* albeit *rigorously parity bound* quantum states with respect to internal rotor predissociation.

This relatively simple observation has significant consequences for Ne–H_2O spectroscopy in both the present VMP overtone efforts and high resolution studies of the bend/stretch fundamentals. To make this simple, let us for the moment neglect any vibrational relaxation effects in the H_2O subunit. By simple parity and B-type dipole selection rules, this means that *para*-Ne–H_2O $|02^+\rangle \leftarrow |00^+\rangle$ excitation out of the ground $\Sigma^e(0_{00})$ state will support allowed transitions to both bound [i.e., $\Pi^f(1_{11})$] and unbound [i.e., $\Pi^e(1_{11})$] upper states on Q and P/R branch transitions, respectively. As parity-allowed internal rotor predissociation is facile, particularly for such a near-resonant system ($\Delta E \approx 2$ cm^{-1}), this would predict (i) highly broadened P/R branch spectra, yet (ii) instrumentally narrow Q-branch transitions. Indeed, spectroscopy and predissociation dynamics of exactly this sort were first noted in high resolution sub-Doppler IR studies of Ne–HF, Ne–DF, He–HF, and He–DF complexes, which revealed instrumentally sharp Q branches and highly broadened P/R branches for $\Pi \leftarrow \Sigma$ internal rotor excitation corresponding to $j_{HF} = 1 \leftarrow 0$ excitation of the monomer.[36] Indeed, extended to He–HCl complexes, the broadening in the P/R branches was so extreme that only the isolated Q-branch structure could be observed, even at high S/N (>20:1).[36]

Though at much lower spectral resolution, the impact of such behavior in the present VMP studies of Ne–H_2O is readily apparent. Specifically, we predict the presence of Q (but not P/R) branch transitions associated with $|02^+\rangle\ \Pi^f(1_{11}) \leftarrow |00^+\rangle\ \Sigma^e(0_{00})$ excitation out of the *para*-Ne–H_2O ground state, with broadening limited fundamentally by slower intramolecular vibrational relaxation of $|02^+\rangle$. These predictions are in fact well confirmed in Fig. 3, specifically with a clear shoulder (7237.00 cm^{-1}) just to the blue of the corresponding $|02^+\rangle\ 1_{11} \leftarrow |00^+\rangle\ 0_{00}$ transition in the free H_2O monomer, and in excellent agreement (ΔE = 0.37 cm^{-1}) with band origin predictions from *ab initio* calculations. Finally, it is worth emphasizing that such good agreement in the VMP action intensities is again consistent with a robust and common intracluster predissociative relaxation pathway, when energetically accessible, from $|02^{\pm}\rangle$ states to a distribution of near-resonant $\{|01^{\pm}\rangle; v_2 = 2\}$ rotational states of the free H_2O monomer, which in turn are efficiently photolysized at 193 nm to form the high rotational states of the OH photofragment detected experimentally.

VI. SUMMARY

Vibrational overtone spectroscopy and *ortho-para* and *e/f parity*-dependent predissociation dynamics of weakly bound bimolecular Ne–H_2O clusters have been probed for the first time by vibrationally mediated photolysis (VMP) methods in a supersonic jet, based on infrared excitation of the first OH stretch overtone ($v_{OH} = 2 \leftarrow 0$) polyad for OH stretching in the water moiety. High level *ab initio* calculations of the Ne–H_2O intermolecular potential energy surface have been performed with coupled-cluster methods [CCSD(T)-f12b/VnZ (n = 3, 4)] and correlation consistent basis sets (VTZ/VQZ), explicitly correlated electron methods, with values corrected for basis set superposition error (BSSE) and extrapolated to the complete basis set (CBS) limit. These *ab initio* theoretical calculations have permitted unambiguous assignment of multiple $v_{OH} = 2 \leftarrow 0$ overtone/internal rotor bands in the *ortho*-Ne–H_2O VMP action spectrum, as well as simple physical explanation for the absence of bands due to rapid nuclear spin state symmetry-dependent predissociation dynamics in the corresponding *para*-Ne–H_2O species. Most importantly, the *ab initio* calculations provide first principles predictions for line-by-line spectra, which are in remarkably good agreement with the experimental band contours.

Furthermore, we observe a surprising dependence of the vibrational predissociation dynamics on *ortho*/*para* nuclear spin symmetry, which can be cleanly interpreted based on a simple physical model of energetically accessible and inaccessible states along the predissociation pathway. Finally, we see direct evidence in the VMP spectra for novel *e*/*f* parity-dependent predissociation dynamics in the $|02^+\rangle\Pi^{e/f}(1_{11})$ internal rotor levels, which can again be explained according to a simple model for parity *blocked* $[\Pi^f(1_{11})]$ vs. *unblocked* $[\Pi^e(1_{11})]$ predissociative access to the asymptotic e-parity $|02^+\rangle$ 0_{00} state of the free H_2O monomer. The results reveal a surprising wealth of novel overtone spectroscopy and dynamics in a prototypical weakly bound van der Waals cluster, whose successful analysis both has clearly been facilitated by and indeed demands close collaborative interaction between experiment and high level theory.

ACKNOWLEDGMENTS

This work was supported by grants from the Department of Energy, Office of Basic Energy Sciences (No. DE-FG02-09ER16021), with additional funds for photolysis laser and construction of the vacuum chamber provided by the Air Force Office of Scientific Research (No. FA9550-12-1-0139). A.v.d.A. and D.J.N. both wish to gratefully acknowledge additional assistance through the Senior Alexander von Humboldt Research Award program for providing the opportunity to work together.

[1] A. Lannung, J. Am. Chem. Soc. **52**, 68–80 (1930).
[2] K. Autumn, M. Sitti, Y. C. A. Liang, A. M. Peattie, W. R. Hansen, S. Sponberg, T. W. Kenny, R. Fearing, J. N. Israelachvili, and R. J. Full, Proc. Natl. Acad. Sci. U. S. A. **99**, 12252–12256 (2002).
[3] A. Bagno, J. Chem. Soc., Faraday Trans. **94**, 2501–2504 (1998).
[4] N. Kobko, M. Marianski, A. Asensio, R. Wieczorek, and J. J. Dannenberg, Comput. Theor. Chem. **990**, 214–221 (2012).
[5] A. Nicholls, K. A. Sharp, and B. Honig, Proteins **11**, 281–296 (1991).
[6] R. C. Cohen and R. J. Saykally, J. Chem. Phys. **98**, 6007–6030 (1993).
[7] R. Lascola and D. J. Nesbitt, J. Chem. Phys. **95**, 7917–7932 (1991).
[8] J. Makarewicz, J. Chem. Phys. **129**, 184310 (2008).
[9] D. Hou, Y. T. Ma, X. L. Zhang, and H. Li, J. Mol. Spectrosc. **330**, 217–227 (2016).
[10] R. E. Grisenti, W. Schollkopf, J. P. Toennies, G. C. Hegerfeldt, T. Kohler, and M. Stoll, Phys. Rev. Lett. **85**, 2284–2287 (2000).
[11] G. Frost and V. Vaida, J. Geophys. Res.: Atmos. **100**, 18803–18809, https://doi.org/10.1029/95jd01940 (1995).
[12] H. G. Kjaergaard, T. W. Robinson, D. L. Howard, J. S. Daniel, J. E. Headrick, and V. Vaida, J. Phys. Chem. A **107**, 10680–10686 (2003).
[13] Z. C. Kramer, K. Takahashi, V. Vaida, and R. T. Skodje, J. Chem. Phys. **136**, 164302 (2012).
[14] K. Takahashi, Z. C. Kramer, V. Vaida, and R. T. Skodje, Phys. Chem. Chem. Phys. **9**, 3864–3871 (2007).
[15] V. Vaida, J. Chem. Phys. **135**, 020901 (2011).
[16] V. Vaida, H. G. Kjaergaard, and K. J. Feierabend, Int. Rev. Phys. Chem. **22**, 203–219 (2003).
[17] S. A. Nizkorodov, M. Ziemkiewicz, D. J. Nesbitt, and A. E. W. Knight, J. Chem. Phys. **122**, 194316 (2005).
[18] P. G. Sennikov, S. K. Ignatov, and O. Schrems, ChemPhysChem **6**, 392–412 (2005).
[19] S. D. Flynn, D. Skvortsov, A. M. Morrison, T. Liang, M. Y. Choi, G. E. Douberly, and A. F. Vilesov, J. Phys. Chem. Lett. **1**, 2233–2238 (2010).
[20] Y. A. Dyadin, E. G. Larionov, A. Y. Manakov, F. V. Zhurko, E. Y. Aladko, T. V. Mikina, and V. Y. Komarov, Mendeleev Commun. **9**(5), 209–210 (1999).
[21] M. P. Ziemkiewicz, C. Pluetzer, M. Wojcik, J. Loreau, A. van der Avoird, and D. J. Nesbitt, J. Chem. Phys. **146**, 104204 (2017).
[22] M. P. Ziemkiewicz, C. Pluetzer, D. J. Nesbitt, Y. Scribano, A. Faure, and A. van der Avoird, J. Chem. Phys. **137**, 084301 (2012).
[23] A. van der Avoird and D. J. Nesbitt, J. Chem. Phys. **134**, 044314 (2011).
[24] M. J. Weida and D. J. Nesbitt, J. Chem. Phys. **110**, 156–167 (1999).
[25] G. T. Fraser, F. J. Lovas, R. D. Suenram, and K. Matsumura, J. Mol. Spectrosc. **144**, 97–112 (1990).
[26] D. F. Plusquellic, O. Votava, and D. J. Nesbitt, J. Chem. Phys. **101**, 6356–6358 (1994).
[27] J. Van Wijngaarden and W. Jager, Mol. Phys. **98**, 1575–1588 (2000).
[28] M. J. Weida and D. J. Nesbitt, J. Chem. Phys. **106**, 3078–3089 (1997).
[29] J. P. Lei, Y. Z. Zhou, D. Q. Xie, and H. Zhu, J. Chem. Phys. **137**, 224314 (2012).
[30] M. P. Hodges, R. J. Wheatley, and A. H. Harvey, J. Chem. Phys. **117**, 7169–7179 (2002).
[31] S. Li, R. Zheng, Y. Zhu, and C. X. Duan, J. Chem. Phys. **135**, 134304 (2011).
[32] X. Sun, Y. Hu, and H. Zhu, J. Chem. Phys. **138**, 204312 (2013).
[33] J. M. Brown, J. T. Hougen, K. P. Huber, J. W. C. Johns, I. Kopp, H. Lefebvrebrion, A. J. Merer, D. A. Ramsay, J. Rostas, and R. N. Zare, J. Mol. Spectrosc. **55**, 500–503 (1975).
[34] C. Chin, R. Grimm, P. Julienne, and E. Tiesinga, Rev. Mod. Phys. **82**, 1225–1286 (2010).
[35] G. Ewing, Chem. Phys. **29**, 253–270 (1978).
[36] C. M. Lovejoy and D. J. Nesbitt, J. Chem. Phys. **93**, 5387–5407 (1990).
[37] C. M. Lovejoy and D. J. Nesbitt, J. Chem. Phys. **94**, 208–223 (1991).
[38] A. K. Mollner, B. E. Casterline, L. C. Ch'ng, and H. Reisler, J. Phys. Chem. A **113**, 10174–10183 (2009).
[39] O. Votava, D. F. Plusquellic, and D. J. Nesbitt, J. Chem. Phys. **110**, 8564 (1999).
[40] D. F. Plusquellic, O. Votava, and D. J. Nesbitt, J. Chem. Phys. **107**, 6123 (1997).
[41] S. A. Nizkorodov, M. Ziemkiewicz, T. L. Myers, and D. J. Nesbitt, J. Chem. Phys. **119**, 10158–10168 (2003).
[42] H.-J. Werner, P. J. Knowles, R. Lindh, F. R. Manby, M. Schütz, P. Celani, T. Korona, A. Mitrushenkov, G. Rauhut, T. B. Adler, R. D. Amos, A. Bernhardsson, A. Berning, D. L. Cooper, M. J. O. Deegan, A. J. Dobbyn, F. Eckert, E. Goll, C. Hampel, G. Hetzer, T. Hrenar, G. Knizia, C. Köppl, Y. Liu, A. W. Lloyd, R. A. Mata, A. J. May, S. J. McNicholas, W. Meyer, M. E. Mura, A. Nicklaß, P. Palmieri, K. Pflüger, R. Pitzer, M. Reiher, U. Schumann, H. Stoll, A. J. Stone, R. Tarroni, T. Thorsteinsson, M. Wang, and A. Wolf, MOLPRO, version 2009.1, a package of *ab initio* programs, 2009, see http://www.molpro.net.
[43] K. A. Peterson, T. B. Adler, and H.-J. Werner, J. Chem. Phys. **128**, 084102 (2008).
[44] K. A. Peterson, R. A. Kendall, and T. H. Dunning, J. Chem. Phys. **99**, 1930–1944 (1993).
[45] K. A. Peterson, D. E. Woon, and T. H. Dunning, J. Chem. Phys. **100**, 7410–7415 (1994).
[46] J. Loreau, J. Lievin, Y. Scribano, and A. van der Avoird, J. Chem. Phys. **141**, 224303 (2014).
[47] J. Tennyson, N. F. Zobov, R. Williamson, O. L. Polyansky, and P. F. Bernath, J. Phys. Chem. Ref. Data **30**, 735 (2001).
[48] M. S. Child, Acc. Chem. Res. **18**, 45–50 (1985).
[49] M. S. Child and R. T. Lawton, Faraday Discuss. Chem. Soc. **71**, 273 (1981).
[50] P. Andresen, V. Beushausen, D. Hausler, H. W. Lulf, and E. W. Rothe, J. Chem. Phys. **83**, 1429–1430 (1985).
[51] V. Engel, V. Staemmler, R. L. Vanderwal, F. F. Crim, R. J. Sension, B. Hudson, P. Andresen, S. Hennig, K. Weide, and R. Schinke, J. Phys. Chem. **96**, 3201–3213 (1992).
[52] D. Hausler, P. Andresen, and R. Schinke, J. Chem. Phys. **87**, 3949–3965 (1987).
[53] R. Schinke, V. Engle, P. Andresen, D. Hausler, and G. G. Balintkurti, Phys. Rev. Lett. **55**, 1180–1183 (1985).
[54] R. Schinke, R. L. Vanderwal, J. L. Scott, and F. F. Crim, J. Chem. Phys. **94**, 283–288 (1991).
[55] V. Engel, R. Schinke, and V. Staemmler, J. Chem. Phys. **88**, 129–148 (1988).
[56] J. Finzi, F. E. Hovis, V. N. Panfilov, P. Hess, and C. B. Moore, J. Chem. Phys. **67**, 4053–4061 (1977).